Manuscript Details

Manuscript number	COGEL_2018_806
Title	Gas storage potential and electrohydraulic discharge (EHD) stimulation of coal seam interburden from the Surat Basin
Article type	Research Paper

Abstract

This paper evaluates the potential methane storage capacity of six clay-rich interburden rock samples from coal seam gas (CSG) wells in the Surat Basin, Australia. Clay minerals identified in all samples included kaolinite, illite, smectite, and illite-smectite mixed-layers. The total organic carbon concentrations in these interburden rocks ranged from 0.66 - 1.19 wt%, and thus these rocks can be classified as fair to good hydrocarbon source rocks. The effective porosity of the rocks determined from mercury intrusion porosimetry and helium pycnometry ranged from 6.8 % to 12.5 %, and included volumes of micropores and mesopores. The adsorption isotherm results indicated that the average adsorption capacity of six interburden was 3.64 cm3/g, a value corresponding to approximately 20% that of Surat Basin coal. Based on the clay compositions and porosity of the samples, the permeability of these Surat interburden rocks is estimated to be less than 5 nano Darcy using Yang and Aplin's empirical correlation, which was too low for reliable measurement in our laboratory core flooding apparatus even with a differential pressure of 10 bar applied over a shortened 20 mm length core. However, after stimulation by electrohydraulic discharge (EHD) shockwaves the permeability of one of the interburden samples (S2) increased to 0.6 ± 0.11 mD due to development of fractures and new pores by the EHD stimulation. We characterised the development of the fractures after EHD shockwaves using x-ray computer tomography. The findings of this study suggest that dynamic shockwaves such as those generated by EHD have potential to increase permeability of soft and clay-rich interburden layers in CSG reservoirs and other layered reservoirs. This potentially opens these ultra-tight gas resources to exploitation and recovery.

Keywords	Coal seam gas; interburden; source rock; dynamic shockwaves; permeability

Corresponding Author	Fei Ren
Corresponding Author's Institution	University of Queensland
Order of Authors	Fei Ren, Lei Ge, Arash Arami Niya, Thomas Rufford, Huilin Xing, Victor Rudolph
Suggested reviewers	Mayumi Ito, Weiran Zuo, Xiaoming Wang

Submission Files Included in this PDF

File Name [File Type]

Gas storage potential and EHD stimulation interburden.docx [Manuscript File]

To view all the submission files, including those not included in the PDF, click on the manuscript title on your EVISE Homepage, then click 'Download zip file'.

Research Data Related to this Submission

There are no linked research data sets for this submission. The following reason is given:
Data will be made available on request

Gas storage potential and electrohydraulic discharge (EHD) stimulation of coal seam interburden from the Surat Basin

Fei Ren[a,b], Lei Ge[c], Arash Arami-Niya[a, †], Thomas E. Rufford[a], Huilin Xing[b], Victor Rudolph[a, *]

a. School of Chemical Engineering, The University of Queensland, St Lucia 4072 Australia

b. School of Earth and Environmental Sciences, The University of Queensland, St Lucia 4072 Australia

c. Centre for Future Materials, University of Southern Queensland, Springfield Central, Queensland 4300, Australia

* *Corresponding author* v.rudolph@uq.edu.au

† *A. Arami-Niya's current affiliation is the Fluid Science & Resources Division, School of Mechanical & Chemical Engineering, The University of Western Australia, Crawley 6009* Australia

Highlights

- A suite of coal seam interburden samples from Surat Basin, Australia have been characterized and investigated for gas potential appraisal, the research outcomes indicated the great prospect of interburden for future exploitation.
- After EHD stimulation, the confining-constrained interburden discs were successfully cracked by introducing some newly induced fractures/voidages from micro- to macroscales.
- During the EHD stimulation process, the maximum shock pressure at both radial and axial orientations, which was loaded on testing interburden disc S5, was simultaneously recorded to reveal the philosophy of interburden breakage.
- As a pioneering trial to stimulate interburden under stress-state, EHD was employed on stimulating clay-rich interburden permeability and providing an alternative technique for argillaceous coal-measure rock development.

Abstract

This paper evaluates the potential methane storage capacity of six clay-rich interburden rock samples from coal seam gas (CSG) wells in the Surat Basin, Australia. Clay minerals identified in all samples included kaolinite, illite, smectite, and illite-smectite mixed-layers. The total organic carbon concentrations in these interburden rocks ranged from 0.66 - 1.19 wt%, and thus these rocks can be classified as fair to good hydrocarbon source rocks. The effective porosity of the rocks determined from mercury intrusion porosimetry and helium pycnometry ranged from 6.8 % to 12.5 %, and included volumes of micropores and mesopores. The adsorption isotherm results indicated that the average adsorption capacity of six interburden was 3.64 cm^3/g, a value corresponding to approximately 20% that of Surat Basin coal.

Based on the clay compositions and porosity of the samples, the permeability of these Surat interburden rocks is estimated to be less than 5 nano Darcy using Yang and Aplin's empirical correlation, which was too low for reliable measurement in our laboratory core flooding apparatus even with a differential pressure of 10 bar applied over a shortened 20 mm length core. However, after stimulation by electrohydraulic discharge (EHD) shockwaves the permeability of one of the interburden samples (S2) increased to 0.6 ± 0.11 mD due to development of fractures and new pores by the EHD stimulation. We characterised the development of the fractures after EHD shockwaves using x-ray computer tomography. The findings of this study suggest that dynamic shockwaves such as those generated by EHD have potential to increase permeability of soft and clay-rich interburden layers in CSG reservoirs and other layered reservoirs. This potentially opens these ultra-tight gas resources to exploitation and recovery.

Keywords: Coal seam gas; interburden; source rock; dynamic shockwaves; permeability

1 Introduction

Coal seam gas (CSG), also called coalbed methane (CBM), is an important source of natural gas for the domestic market and liquefied natural gas (LNG) export market in eastern Australia. In the state of Queensland CSG contributes almost 88% of the gas produced and approximately 99% of the remaining proved and probable (2P) gas reserves (Mines, 2015). The primary hydrocarbon targets in CSG wells are the coal layers, but the clay-rich interburden layers found between coal-bearing measures could potentially contain significant volumes of gas in addition to the gas contained in the coal-bearing measures.

For example, in the Surat Basin, an intracratonic basin of early Jurassic to early Cretaceous age covering approximately 300,000 km^2 in eastern Australia, CSG wells are completed across multiple, often thin, gas producing coal seams (Hamilton et al., 2012). The stratigraphic column shows the net thickness of interburden layers is much larger than the net thickness of coal-bearing measures (Bustin and Bustin, 2016; Hamilton et al., 2014; Ryan et al., 2012). These interburden layers consist of carbonaceous mudstone, siltstones, and organic components that can hold methane as adsorbed gas (Scott et al., 2007b). However, currently in most appraisals of CSG reservoirs the contribution of the non-coal interburden facies to stored gas volumes is neglected (Bustin and Bustin, 2016).

The clay constituents acquired from testing Surat interburden were the same as the clays reported from shale samples (Chen et al., 2016; Tang and Fan, 2014), suggesting that the inorganic matter in interburden might play a similar role as it does in shales. The clay minerals in mudrocks were found to be able to have significant gas adsorption capacities due to theie large micropore volumes and specific surface areas which are necessary for adsorbed gas storage (Liu et al., 2013; Ross and Bustin, 2007). In particular, Schettler and Parmoly (Schettler and Parmoly, 1990) stated that, in low kerogen shales, clay minerals can contribute most to methane adsorption capacity. Given the abundance of clay minerals in the interburden, the findings reported here confirm that clay-rich mudrocks, which characterise much of the coal seam interburden, present potential for gas adsorption and storage.

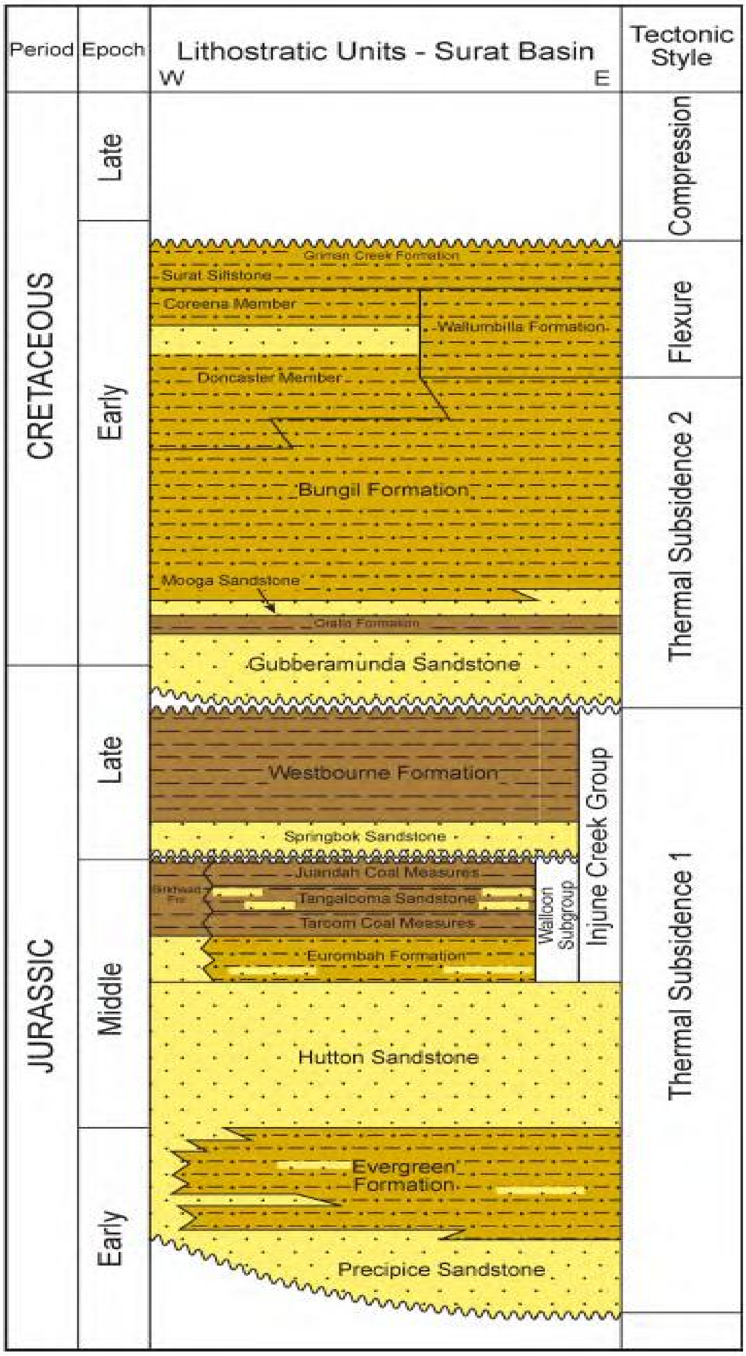

Figure 1 Surat Basin stratigraphic column (Ryan et al., 2012)

Due to the differences in the characteristics of reservoirs, the gas development potential of the interburden is location specific and would need to be assessed at the resource appraisal stage. This seems generally neglected and interburden rocks in coal measures are still one of the least understood of sedimentary rocks (Aylmore, 1973; Neuzil, 1994; Potter et al., 2005; Shneider et al., 2011). Their potential as viable methane sources has not yet been well developed, compared with that of sandstone, coal or shale. Specifically, fundamental questions regarding whether interburden is worth developing as a potential source rock, and if so, what methodology is applicable for its stimulation, are still unanswered.

Primarily, physical properties pertaining to gas development such as clay mineralogy, geometry of pore system, mechanical features, isothermal adsorption capacity, porosity and permeability should be addressed (Dumbleton and West, 1966; Yang and Aplin, 2010). Unfortunately, published articles on interburden characterization remain limited and rare. Most of the existing articles about mud and clay rocks have mainly dealt with typical oil/gas sedimentary basins, and omitting coal seam interburden in coal basins (Ewhurst et al., 1999; Yang and Apin, 2004), They are usually typified for applications such as seal layers in petroleum exploration and production, rather than source rock reservoirs (Ewhurst et al., 1999). While the reservoir characterizations of interburden in petroleum engineering and the geoscience system, which are relevant to gas formation, storage and fluid flow provide some guidance, they are obviously different regarding appraisal for CBM (Gamson et al., 1996; Perera et al., 2010; Ross and Marc, 2009).

Previous interburden research based on other applications suggest that, in general, its permeability can be as low, in the order of nano-Darcy, whereas its compressibility can be high enough to lead to overpressure because of the complex compaction behaviour and diagenesis processes (Broichhausen et al., 2005). The mechanical properties of mudstones tend to show lower Young's Modulus and lower brittleness index compared to conventional sandstone reservoirs or gas shales. This is likely to make them extremely difficult to disaggregate by classic stimulation techniques, namely hydraulic fracturing (Ajalloeian and Lashkaripour, 2000; Mcdaniel, 2005).

Hydraulic fracturing is the most widely used and useful technique to enhance gas production in low permeable but fissile reservoirs such as shales or coal seams. However, the mechanical response of interburden is likely to be quite different from that of fissile reservoirs, as the interburden layer is comprised of more quasi-brittle and clay-rich minerals. Hydraulic fracturing would likely cause severe clay swelling and softening or deformation. Swelling will likely block the throats and occlude cleats when encountering incompatible fracturing fluids (Potter et al., 2005) limiting effectiveness of hydraulic fracturing. Other stimulation techniques such as waterless fracturing has received much attention for unconventional reservoir development; however, so far none of them has been adopted as a proven technique by the industry (Gandossi, 2013; Gandossi, 2016).

This paper focuses on the interburden characterization and the evaluation of its potential as source rock, particularly seeking to address two key parameters affecting commercial exploitation, i.e., gas storage ability and low permeability. Considering the specific features related to gas production, an alternative stimulation method, i.e., electrohydraulic discharge (EHD), which applies dynamic shock loading to stimulate clay-rich interburden and generate comprehensive fracture networks, is developed and validated on a suite of Surat interburden samples. The outcomes show that both the flow conductivity and fractures of interburden can be greatly improved by using EHD stimulation.

2 Experimental methods

2.1 Samples and geological setting

Six core samples, labelled S1 to S6, were collected from interburden layers at depths from 300 to 750 m in Surat Basin CSG wells. Figure 2 shows the rock cores were dark brown, grey or greyish-brown colours, and the visual appearances suggests these are mudrocks with fine clay mineral and organic matter. The major-coal bearing targets for CSG wells in the Surat Basin are in the Walloon subgroup (Ryan et al., 2012). The Hutton Sandstone, Evergreen Formation and the Precipice Sandstone are the major sediments below the Walloon subgroup coals in the Surat Basin (Exon, 1976; Hamilton et al., 2014; Martin et al., 2013).

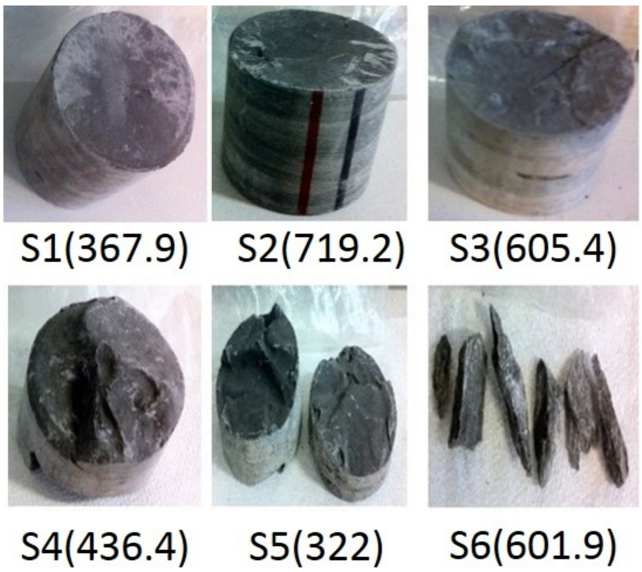

Figure 2 Interburden cores S1 to S6 from Surat Basin, Australia. The number in brackets for each sample shows the depth in metres at which the sample was collected.

2.2 *Sample characterisation methods*

Sections of each core were prepared for thin section analysis; cut into fragments for compositional and porosity characterisation, and high pressure methane adsorption measurements; and cut into 15 mm cubes for strength measurement. Samples S2 and S5 were also cut to 63.5 mm diameter and 20 mm (S2) or 19 mm (S5) length cores for permeability measurements and EHD simulation.

The concentration of organic matter in each sample was estimated from thin sections analysed under a Leica DM 750 microscope and total organic carbon (TOC) was measured on a LECO C-230 carbon analyser. Clay minerals in each sample were identified by X-ray diffraction (XRD, Bruker D8 Advance), and surface elements were determined using energy dispersive x-ray spectroscopy (EDS) on a Hitachi SU3500 premium VP-SEM scanning electron microscope operated at 15 kV. All samples were coated with Au before scanning in the SEM.

The unconfined compressive strength (UCS) of 15 mm cubes cut from the cores was measured on a CT3400-2000KN instrument (Impact Test Equipment Ltd) following standard procedures described in ASTM D7012–14. The bulk or apparent density (ρ_{Hg}) was measured by mercury intrusion porosimetry (MIP, Micromeritics AutoPore IV9520) and the skeletal density (ρ_{He}) by helium pycnometer (Micromeritics AccuPyc II 1340). The porosity (□) was calculated using Eq. (1):

$$\emptyset(\%) = \frac{\rho_{He} - \rho_{Hg}}{\rho_{He}} \times 100 \qquad (1)$$

Nitrogen (N_2) and carbon dioxide (CO_2) sorption isotherms were measured at 77 K and 273 K, respectively, with a TriStar II 3020 apparatus (Micromeritics, USA) after degassing the samples at 473 K under a vacuum pressure of 10^{-5} torr for 24 h. Pore size distributions (PSD) were calculated from the N_2 sorption isotherms using a non-local density functional theory (NLDFT) model supplied in the Tristar II 3020 software. Micropore surface area and limiting micropore volume were determined from CO_2 isotherms using the Dubinin-Astakhov (DA) equation (Saeidi and Parvini, 2015).

High pressure methane adsorption isotherms were measured at 308 K and at pressures up to 8 MPa on a Belsorp-BG apparatus (BEL, Japan) equipped with a magnetic floating balance (Rubotherm, Germany). Details of the Belsorp-BG apparatus and its operation are described in previous articles (Arami-Niya et al., 2017; Arami-Niya et al., 2016). Samples were degassed in situ at 423 K for 24 h before the high pressure adsorption measurements.

Rock cores were scanned, before and after the EHD shock stimulation, in a Siemens Inveon Multimodality PET/CT scanner operated at 80 kV with a beam current of 0.5 mA. The CT images were reconstructed, visualised and regularized on the Inveon™ Research Workplace software (Seimens IRW v4.2) to analyse fracture evolution after EHD stimulation.

2.3 Electrohydraulic discharge stimulation apparatus

The EHD stimulation apparatus shown in Figure 3 consists of (A) a high-voltage pulsed power instrument (Suematsu Inc., MPC3010S-5J); (B) a Keysight DSOX2024A oscilloscope to record the EHD waveform; (C) a Teledyne ISCO 260D syringe pump and (D) pressure transducer (Gems 3200) to control and measure, respectively, the confining fluid pressure on the core sample held in (J) a Hassler-type biaxial core holder (Core Labs, USA); (E) a Fuji pressure film for detecting the shockwave pressure at the leeward end of the core; and (I) a Teledyne ISCO 260D syringe pump, Swagelok tubing, and instrumentation to control and measure the injection fluid flow and pressures. The pulsed power instrument and core holder were connected by high-voltage cables that terminated across a 1 mm gap between two purpose built electrodes placed 1 mm apart and within a parabolic-shaped reflector dish (K). This parabolic disc is used to reflect the produced shockwaves and enhance the core fracking effect (Zhang et al., 2012b). In this configuration the high-voltage pulsed power instrument can generate a voltage of up to 30 kV across the 1 mm electrodes gap.

The 63.5 mm diameter cores cut from samples S2 and S5 were loaded separately into the core holder and held at a confining pressure of 20 bar for 72 hours before permeability measurements or EHD stimulation. Both cores were subjected to 2000 EHD pulses each at a constant charging voltage of U_c=30 kV. The pulse frequency and length of pulse were controlled at 40 pulses per second (PPS) for 50 seconds in the S2 stimulation experiments, and at 80 PPS for 25 seconds in S5 stimulation. The permeability of cores after EHD stimulation was measured without changing the confining stress or removing the core from the core holder.

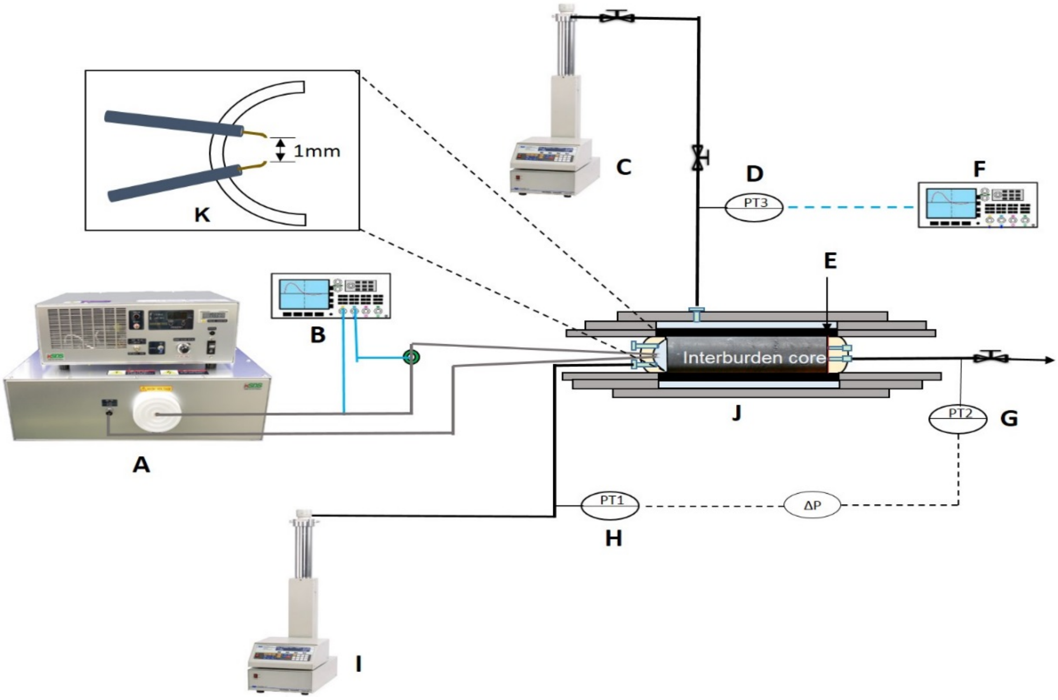

Figure 3 Schematic of compact pulsed power generator with core flooding rig for interburden stimulation. (A) compact pulsed power generator, (B),(F) oscilloscopes, (C) confining pressure pump, (D),(G),(H) pressure transducer, (E) Fuji pressure film, (I) injection pressure pump,(J)core flooding rig,(K)sketch of the electrode design

2.4 Permeability measurements

The permeability of cores was measured with a 4%wt KCL solution before and after EHD stimulation using a steady-state method in the Hassler-type biaxial core flooding apparatus (Figure 3). A differential pressure (ΔP) of approximately 10 bar was applied across the core using the syringe pump (G) to control inlet fluid pressure with the outlet pressure controlled with a back pressure regulator to close to atmospheric pressure. The steady-state permeability was calculated using to Darcy's law:

$$k_w = \frac{Q u_w L}{A \Delta P} \qquad (2)$$

where k_w is permeability in Darcy; Q is the pump flow rate in cm^3/s, u_w is the viscosity of 4% KCL brine which was assumed to be a constant 0.9 mPa•s at our experimental conditions (Grimes et al., 1979); A is the cross-sectional area of each core (31.65 cm^2); L is the length of cores (S5 1.9 cm and S2 2.0 cm); and ΔP is the pressure drop across the core in atmospheres.

3 Results and discussion

3.1 Characterisation of interburden rock samples

3.1.1 Mineral composition

The powder XRD patterns in Figure 4 identify the clay minerals kaolinite, smectite, and illite in each of the six interburden core samples S1 to S6. The XRD patterns of all six samples also contain significant peaks associated with quartz, and we have previously identified that interburden samples from these locations also contain traces of potassium feldspar and goethite (Ge et al., 2018). Further evidence of the presence of illite, smectite, kaolinite, and illite/smectite mixed-layer clay minerals in the interburden samples is provided in the EDS data in Figure 5, and in the SEM images of samples S1 and S2 in Figure 6, which show surface features with morphologies matching that illite/smectite mixed-layers and kaolinite. These XRD, SEM, and EDS results are consistent with the expected compositions of the interburden layers in the Surat Basin.

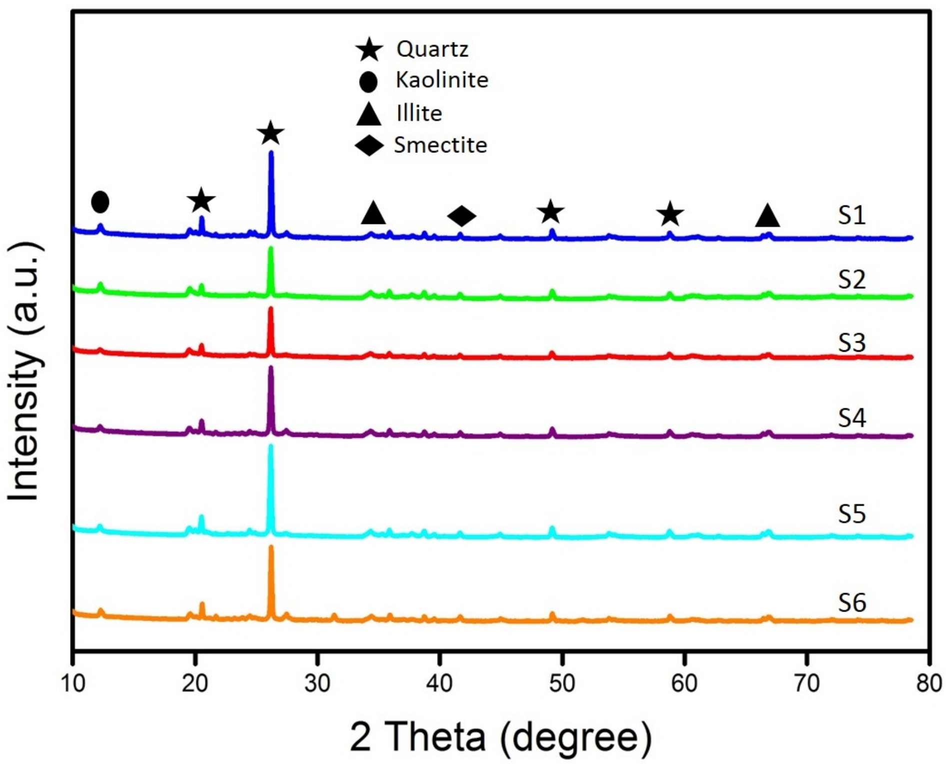

Figure 4 Powder XRD patterns of rock samples S1 to S6 collected from interburden layers in Surat Basin coal seam gas wells.

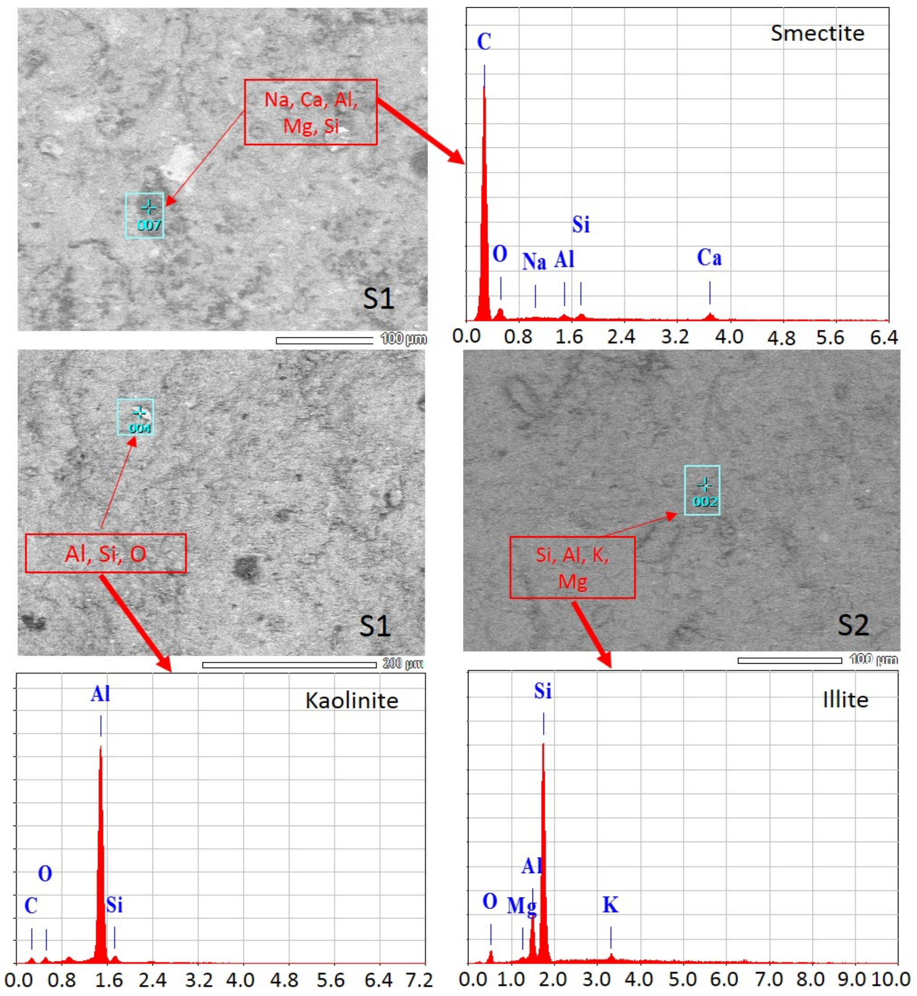

Figure 5 SEM and energy dispersive X-ray spectroscopy (EDS) spectra of smectite, kaolinite, and illite regions in rock samples S1 and S2 collected from interburden layers of a Surat Basin coal seam gas well.

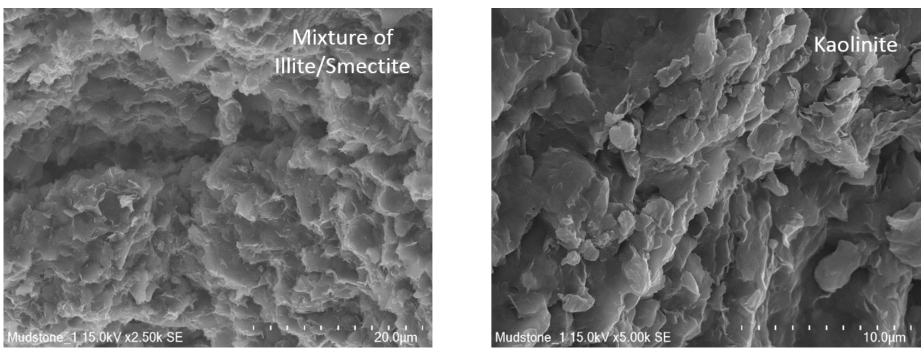

(a) *(b)*

Figure 6 SEM images of the surfaces of rock samples collected from interburden layers in a Surat Basin coal seam gas well. These SEM images are of samples (a) S1 and (b) S2, and are representative of features observed on all six interburden rock samples in this study.

3.1.2 Total organic carbon

The optical microscope images in Figure 7 show regions of organic matter dispersed throughout the clay minerals in thin sections of interburden sample S5. The irregular dark regions were identified as organic matter, while the grey light areas were clay minerals. The total organic carbon (TOC) concentrations in the six interburden samples ranged from 0.67 wt% in S4 to 1.19 wt% in S5, as summarised in Table 1. Based on these TOC concentrations and according to the source rock quality classifications proposed by Bacon et al. (2000), cores S2 and S5 may be classified as good source rocks and the other four cores (S1, S3, S4, S6) may be classified as fair source rocks.

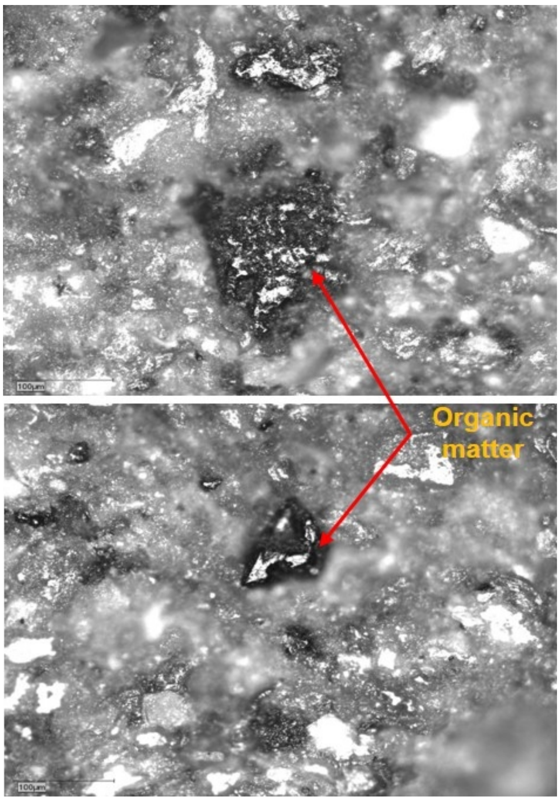

Figure 7 Typical optical microscope photograph of a thin-section of mudrock sample S5 collected from an interburden layer in a Surat Basin coal seam gas well. The dark regions in the image are the organic materials.

Table 1 Total organic carbon content of rock cores from interburden layers in CSG wells in the Surat Basins, Australia

Sample	Organic C (wt%)	Inorganic C (wt%)	Total carbon (wt%)	Source rock classification by Bacon et al. (2000)
S1	0.85	0.34	1.19	Fair
S2	1.11	0.06	1.17	Good
S3	0.8	0.06	0.86	Fair
S4	0.66	<0.02	0.67	Fair
S5	1.19	0.12	1.31	Good
S6	0.86	<0.02	0.87	Fair

3.1.3 Uniaxial compression test

The unconfined compressive strength of 15 mm cubes cut from S2 and S5 was measured to provide mechanical rock properties that can be used to develop stimulation operations (Bieniavski, 1968; Rao et al., 2015). Figure 8 shows samples S2 and S5 failed at compressive strengths of 27.6 MPa and 22.1 MPa, respectively. These two interburden rocks have much higher compressive strength than Queensland coals which have been measured in our laboratory, for example typically failure points for New Acland coals are in the range 11.5 - 18.1 MPa. These UCS results suggest that fracturing of interburden may be more difficult than fracturing of coal.

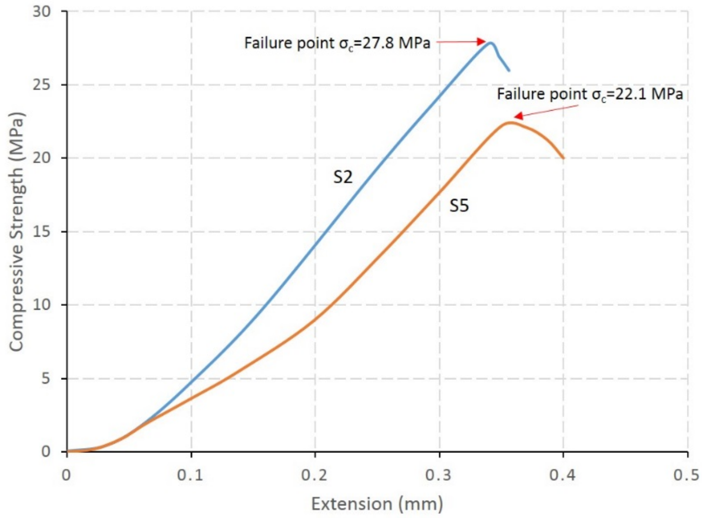

Figure 8 Uniaxial stress-extension curves of 15 mm cubes of samples S2 and S5 interburden.

3.1.4 Porosity and pore characterisation

The bulk and skeletal densities listed in Table 2 for each of the six samples of Surat Basin interburden layers are within the typical range of densities expected for siltstones and mudstones (1.9 g/cm^3 to 2.6 g/cm^3) (Burra and Esterle, 2011). The total effective porosities of the Surat Basin interburden samples were in the range from 6.8 % (S5) to 12.5 % (S3). A total effective porosity could not be calculated for S4 because the measured ρ_{Hg} was greater than ρ_{He} for this sample; this anomaly is likely due to small variations between the sectioned samples used for the helium and MIP measurements, and the uncertainties in measurements of ρ_{Hg} and ρ_{He}. There are few publically available reports of porosities for Surat Basin interburden rocks to compare these result to; only one public document by QGC (now Shell) was found, reporting porosities from 3% to 26% in Surat Basin interburden cores which indicates a large variability in porosity across interburden layers in the Surat Basin. The 6.8 - 12.5 % total effective porosity of the samples as measured for this work was of a similar magnitude to the total effective porosity of coals from the Bowen Basin (Ramandi et al., 2016).

Table 2 Skeletal density ρ_{He} determined from helium pycnometer, bulk (apparent) density ρ_{Hg} determined from mercury intrusion porosimetry (MIP), and total effective porosity □ of mudrock samples collected from coal seam gas wells in the Surat Basin. A total effective porosity for S4 could not be calculated because the measured ρ_{Hg} was greater than ρ_{He} for this sample (Experimental uncertainties forρ_{He} and ρ_{Hg} are below 0.01 g/cm3)

Sample	ρ_{He} (g/cm^3)	ρ_{Hg} (g/cm^3)	Total effective porosity (%)
S1	2.66	2.35	11.7±0.9
S2	2.66	2.35	11.7±0.7
S3	2.63	2.30	12.5±1.1
S4	2.65	2.76	–
S5	2.64	2.46	6.8±0.6
S6	2.61	2.34	10.3±0.8

Figure 9 presents (a) cumulative pore volume distributions and (b) incremental pore size distributions (PSD) of the six interburden samples determined from mercury intrusion porosimetry. The cumulative intrusion volumes ranged from 0.031 cm^3/g in S3 to 0.057 cm^3/g (Figure 9a). The PSDs in Figure 9b show two regions of pore widths in the interburden samples: (i) a large volume of mesopores (widths 0.001 – 0.025 µm on the Figure 9b axis) and small macropores (widths up to 0.1 µm), and (ii) a smaller volume of fractures and large apertures with widths 20 – 100 µm. Generally, this type of PSD tendency is common for clay-rich shaly rocks (Zhang et al., 2012a). For example, the bimodal PSDs in Figure 9b have similar features to PSDs in Devonian-Mississippian shale samples reported by Ross and Bustin (2009).

There are a mix of Type II and Type IV shaped isotherms (Sing et al., 1985) in the N_2 sorption isotherms measured at 77 K in Figure 10a. The Type II continually increasing isotherm is characteristic of a material with a broad pore size distribution range, which is consistent with the MIP results. The hysteresis loops of the Type IV component of the isotherm at relative pressures ranging from around P/P_0=0.5 to P/P_0=0.9 can be associated with capillary condensation in mesopores (Sing et al., 1985), and this result is also consistent with the MIP derived PSD in Figure 9b. For all these interburden rocks, a steep increase of adsorbed N_2 volume was observed at relative pressures approaching $P/P_0 = 1$, which is attributed to filling of large pores with condensed N_2. The total volume of N_2 adsorbed on the interburden samples at P/P_0=0.995 varies from 22.7 cm^3/g on S6 to 33.1 cm^3/g on S3. It may be noted that these N_2 adsorption capacities are greater than some reported N_2 volumes of around 14 cm^3/g on coals from Pennsylvanian (Mastalerz et al., 2012)and Jiulishan (Qi et al., 2017).

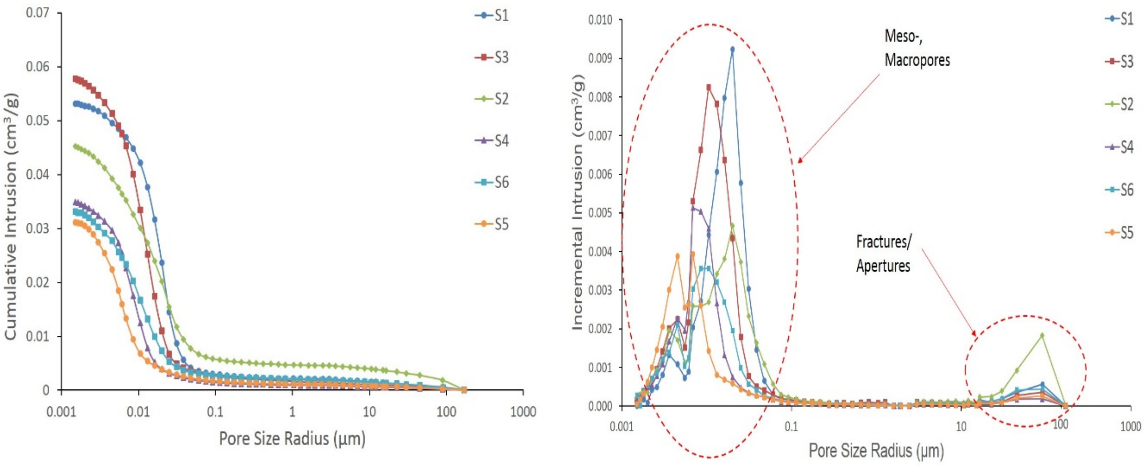

(a) *(b)*

Figure 9 (a) Cumulative pore volume and (b) incremental pore size distribution determined by mercury intrusion porosimetry in interburden samples from CSG wells in the Surat Basin.

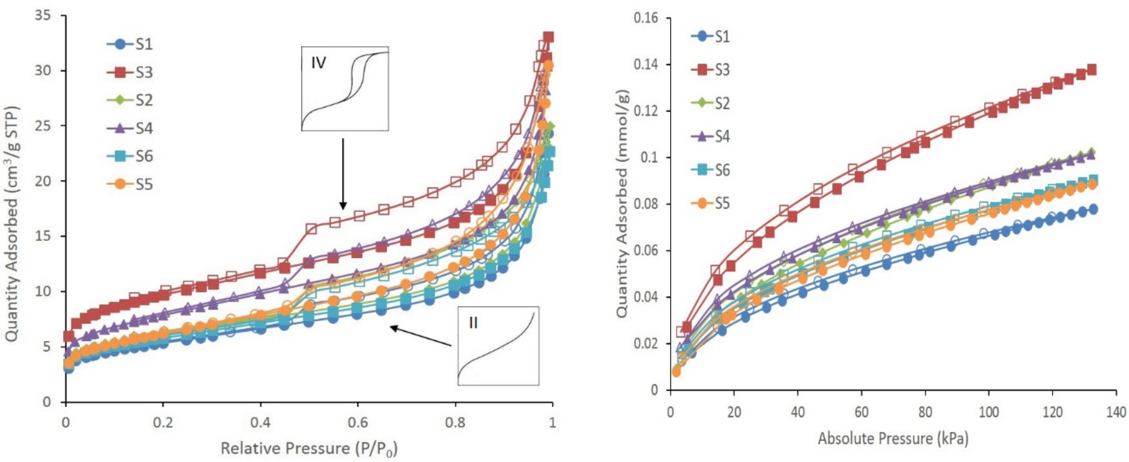

(a) *(b)*

Figure 10 Adsorption isotherms of (a) N_2 at 77 K and (b) CO_2 at 273 K for interburden samples.

Table 3 summarizes the pore textural properties of the six interburden samples derived from the 77 K N_2 isotherms (Figure 10 a) and the 273 K CO_2 isotherms (Figure 10 b). The Brunauer-Emmett-Teller (BET) specific surface area of the six interburden samples vary from S1 18.98 m^2/g to S3 34.35 m^2/g, and the total pore volumes range from S6 0.034 cm^3/g to S3 0.050 cm^3/g. The trends in N_2 adsorption results were consistent with the MIP data and total effective porosities with S3 having the highest pore volume measured by N_2 sorption. The surface areas calculated by CO_2 isotherms with the Dubinin-Astakhov (DA) method are 5 – 10 m^2/g greater than the BET surface areas and the DA micropore volumes are slightly less than the sum of micropore and macropore volumes calculated from the N_2 isotherms. These minor differences are not significant, and can be expected due to the different measurement conditions, relative pressure ranges, and kinetic limitations in the N_2 sorption measurements (Ghosal and Smith, 1996).

Figure 11 shows the PSD of the six interburden samples determined by NLDFT from the N_2 sorption isotherms. The PSD curves reveal micropores (<2 nm) in these rocks, with the increment pore volume starting from 0.0003 cm^3/g in S5 to 0.0007 cm^3/g in S3. The range of micropore volums in the Surat Basin interburden samples are similar to the pore volumes in the Pennsylvanian coal (0.0006 cm^3/g) and Upper Devonian-Mississippian shale samples (<0.0002 cm^3/g) reported by Mastalerz et al. (2012), which may indicate the gas storage potential of the interburden is similar to those coals and shale rocks.

Table 3 Summary of pore textural properties of interburden samples. BET specific surface area, total pore volume at P/Po=0.98 and micropore and mesopore volume determined from N2 sorption at 77 K. Dubinin-Astakhov (DA) micropore surface area and limiting micropore volume determined from CO2 adsorption isotherms at 273 K.

Sample	N_2 adsorption			CO_2 adsorption	
	S_{BET} (m^2/g)	V_{total} (cm^3/g)	$V_{micro}+V_{meso}$ (cm^3/g)	S_{D-A} (m^2/g)	V_{micro} (cm^3/g)
S1	18.98	0.036	0.018	32.01	0.018
S2	21.82	0.037	0.016	31.45	0.015
S3	34.35	0.050	0.030	47.36	0.025
S4	28.06	0.046	0.022	31.31	0.016
S5	22.23	0.046	0.023	27.85	0.014
S6	20.68	0.034	0.020	31.11	0.016

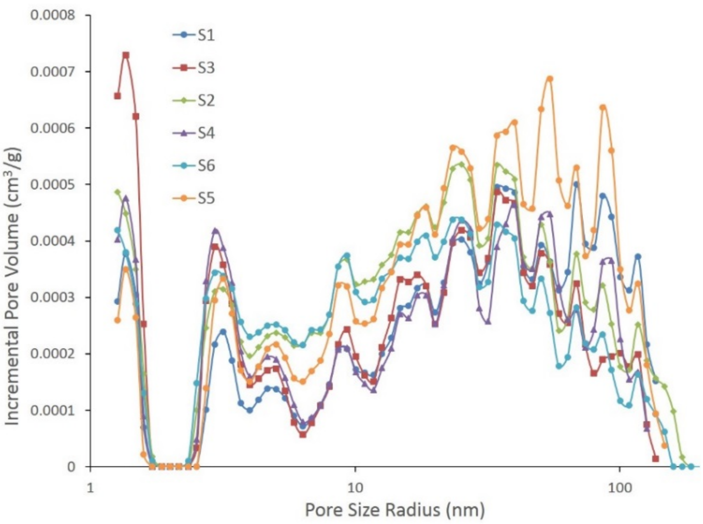

Figure 11 Pore size distribution of micropores and mesopores in core samples from interburden layers in CSG wells in the Surat Basin determined by NLDFT from the N_2 sorption isotherm measured at 77 K.

3.1.5 Methane adsorption capacity

Absolute equilibrium adsorption capacities of CH_4 at 308 K and pressures up to 8 MPa on the six Surat Basin interburden samples in this study are shown in Figure 12a. These results are adsorption capacities measured in the laboratory and should not be confused with the actual gas content in the reservoir as measured by gas desorption tests from preserved cores. The sample depth in metres relative to the drilling rig is indicated next to each isotherm.

Although it may be observed in Figure 12a that CH_4 adsorption capacity increases with depth, it is important to note that this depth is only relative to the drilling rig at each well and no attempt has been made to correlate sample collection depths in the different wells to geological layers across the Surat Basin. Instead, the main insights from Figure 12a relate to the physical properties of the rock that are influenced by depth and depositional environment: such as TOC, clay content, mineral composition, moisture, and porosity (Guo and Guo, 2017; Ross and Bustin, 2007; Scott, 2008). The trends between CH_4 capacity at P=8 MPa and some of these properties are explored in Figure 12 parts b, c, and d. These figures show higher CH_4 adsorption capacities in samples with higher TOC concentrations (Figure 12b), with higher total effective porosity (Figure 12c), and with greater micropore volume (Figure 12d). These general trends are consistent with other studies of gas adsorption capacities in porous clay-rich and shaley rocks (Ross and Bustin, 2007; Yu et al., 2014).

The Langmuir isotherm model (Langmuir, 1918), in Equation 3, is convenient to predict the measured adsorption capacities on each interburden sample:

$$V = \frac{V_L \times P}{P_L + P} \quad (3)$$

where V (cm^3/g) is the adsorbed gas volume at pressure P (MPa), and V_L and P_L are regression parameters.

The best-fit parameters for Equation 3 determined by a least-squares regression analysis are listed in Table 4, and compared to a summary of typical ranges of values for V_L and P_L summarised by Scott et al. (2007a) literature survey of 86 coals from the Walloon Subgroup of Surat Basin. This comparison shows that the potential CH_4 storage capacity in the Surat Basin interburden samples in our study are about 20 % of the CH_4 capacity of Walloon Subgroup coals. Although the specific gas capacity of the interburden measured here is less than for the coals, the total volume of gas potentially stored in interburden layers may be comparable to total volumes in coal layers in locations where the cumulative thickness of interburden layers is ten times that the target coal measures (Bustin and Bustin, 2016). The interburden rocks studied in this paper may be porous and show considerable potential gas storage capacity, but as discussed in Sections 3.2 and 3.3 the very low permeability of these rocks needs to be enhanced for economically viable extraction of any accumulated gas from the interburden layers.

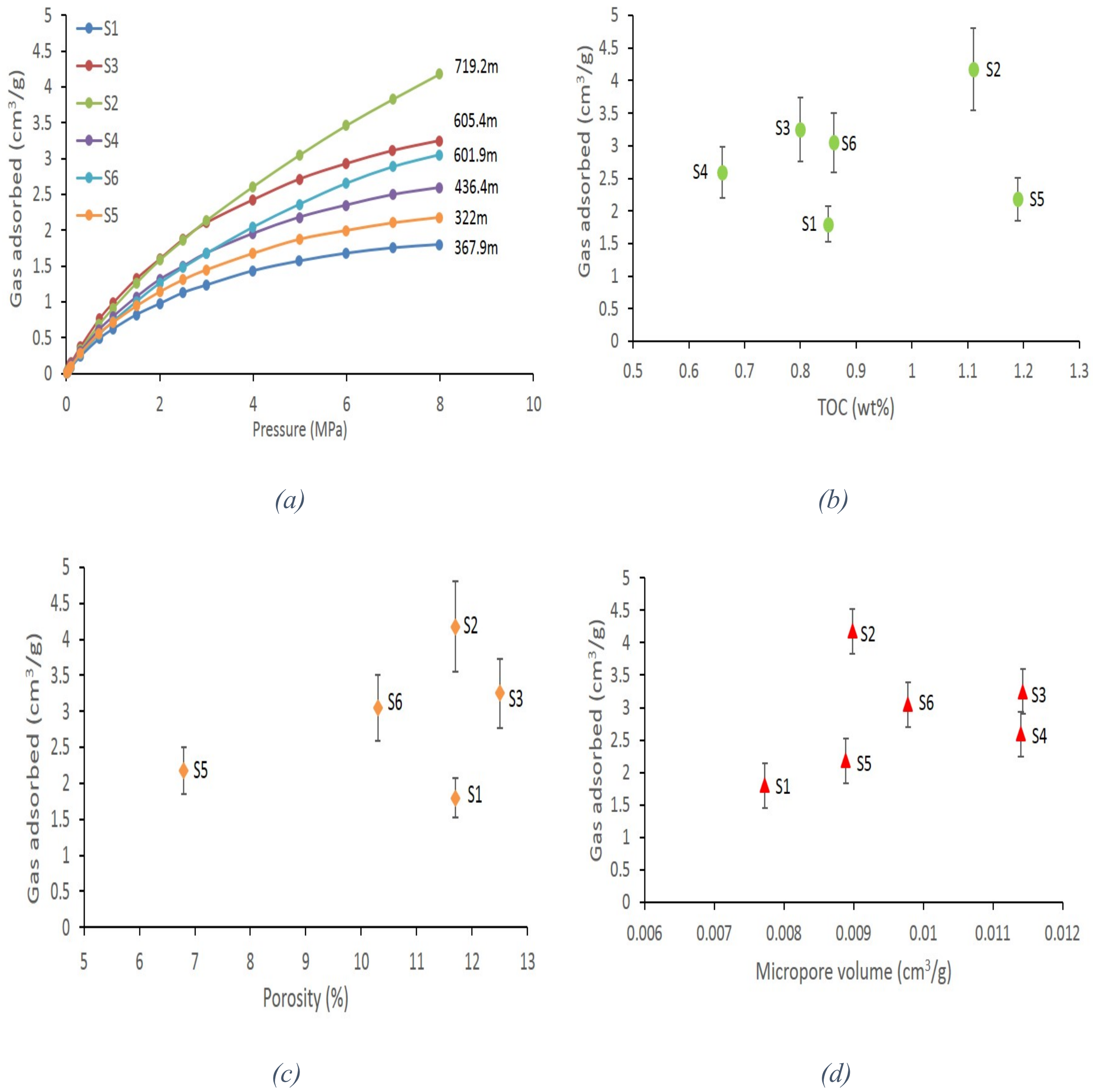

Figure 12 (a) Absolute adsorption capacities of CH_4 on core samples from interburden layers in CSG wells in the Surat Basin measured at 308K; and adsorbed gas volume (cm^3/g) at P=8 MPa versus (b) TOC (wt%), (c) porosity (%) and (d) micropore volume (cm^3/g)

Table 4 Best fit parameters for Langmuir isotherm model Langmuir volume and pressure for six Surat interburden at a measurement temperature of 308K and an example of the range of Langmuir parameters for Walloon Subgroup coals reported in the literature

Sample	V_L(cm^3/g)	P_L(MPa)
S1	2.12	1.41
S2	6.21	3.89
S3	3.76	1.25
S4	3.14	1.68
S5	2.58	1.46
S6	4.06	2.65
Walloon Subgroup coal, typical values (After Scott et al., 2007a)	3.88~25.10	0.91~12.81

3.2 Estimate of interburden permeability before EHD stimulation

An attempt was made to measure the permeability of cores S5 and S2 in the Hassler-type biaxial core flooding apparatus before EHD stimulation. However, the permeability of these two mudrocks was so low that even with a 10 bar pressure drop across a 20 mm core length there was insufficient liquid passed through the core after 7 hours to get a measureable permeability. As an alternative approach to estimate the permeability of the interburden rocks before EHD stimulation , the Yang and Aplin (2010) empirical correlation was used:

$$\ln(k) = -69.59 - 26.79 \times CF + 44.07 \times CF^{0.5} + (-53.61 - 80.03 \times CF + 132.78 \times CF^{0.5}) \times \varepsilon \\ + (86.61 + 81.91 \times CF - 163.61 \times CF^{0.5}) \times \varepsilon^{0.5} \quad (4)$$

where k is the permeability in the direction perpendicular to the bedding plane (in units of m^2); ε is the void ratio ($\varepsilon = \emptyset/(1-\emptyset)$); and CF is the fraction of clay in the rock.

The orange shaded box in Figure 13 presents the range of permeability values predicted with Equation 4 for the six Surat Basin interburden samples based on: (1) the limits of CF between 30 – 90 % described in Yang and Apin (2004), because there was no direct measurement of clay content (only qualitative XRD analysis); and (2) the minimum (6.8%, S6) and maximum (12.5%, S3) measured total effective porosities of the six samples. Using these parameters, the estimated permeability of the interburden samples is in the nano-Darcy range (1.19 x 10^{-7} mD to 1.02E x 10^{-5} mD), which is similar to the range of permeabilities for interburden rocks reported by Neuzil (1994). These calculated permeabilities also fall within the range of mudrock permeabilities reported by QGC (now Shell) for other rocks from their CSG tenements included on Figure 13.

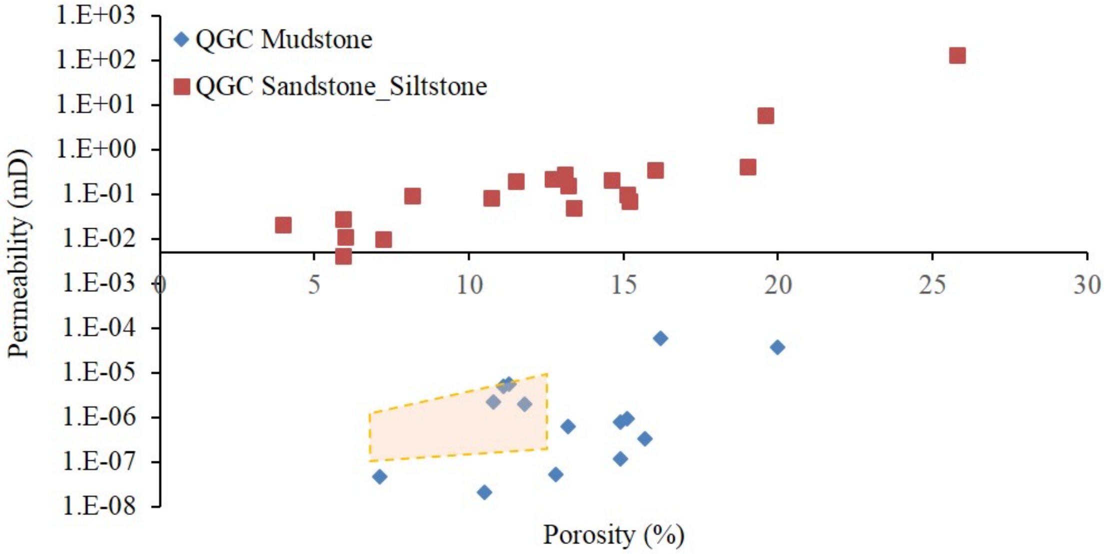

Figure 13 Estimated range of permeability of Surat Basin interburden samples (yellow shaded area) based on Yang and Aplin's correlation using measured porosity range and clay content range from 30 – 90 %. Examples of actual measured permeability of other cores from Surat Basin including mudstones and sandstone-siltstone rich cores.

3.3 Electrohydraulic discharge stimulation of interburden

Figure 14 presents two types of waveforms observed with different breakdown voltage responses during EHD stimulation of interburden cores at an initial charging voltage U_c = 30 kV. In the N shaped waveforms (Figure 14 a) the voltage drops from 30 kV to U_b = 26.5 kV over a 3 μs breakdown time delay. In contrast, in the A shaped waveform (Figure 14 b) there is an almost instantaneous breakdown at U_b = 30 kV. Both N and A types were observed in the experiments with both S2 and S5 cores. Generally in EHD processes, the energy transformation from electrical discharge to shockwave generation is more efficient when the breakdown voltage is closer to initial charging voltage (Yan et al., 2016b), and thus it may be expected that A shaped waveform is likely to lead to a more efficient stimulation and rock fracturing process. With the repeated shockwave generation, the discharging water and interburden properties could change gradually, for instance detached rock particles mixed into discharging water, thus in turn both the discharging electrolyte and loading resistance and/or conductivity could change during the EHD stimulation and these changes may affect the breakdown voltage and waveform shape even if U_c is kept constant.

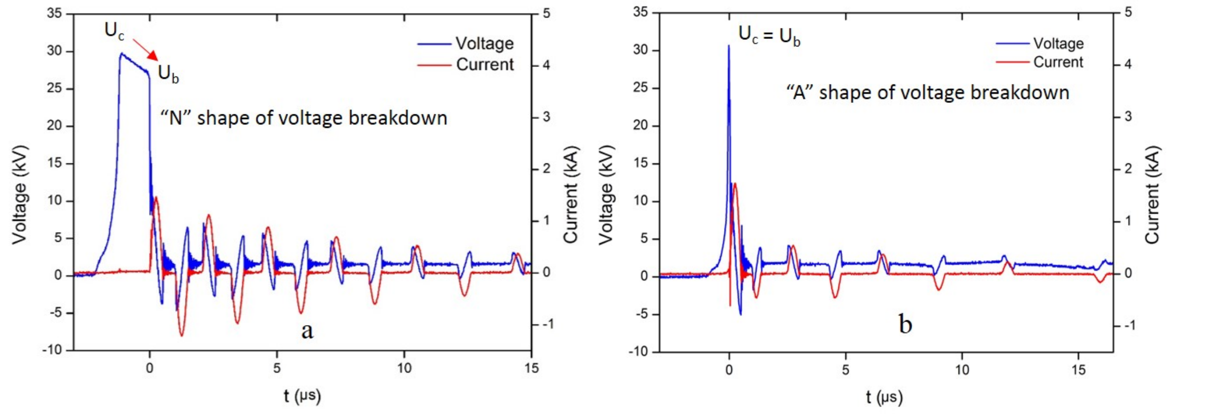

Figure 14 Two typical types of waveforms recorded during EHD stimulation of interburden cores with initial charging voltage U_c = 30 kV. (a) N shaped voltage breakdown waveform and (b) A shaped voltage breakdown.

After EHD stimulation the permeability of S2 increased several orders of magnitude from less than 5 nano Darcy to 0.6 ± 0.11 mD (Figure 15). The 3D x-ray CT derived voids maps in Figure 16a show before EHD stimulation core S2 had no visible fractures extending to the external surfaces of the core, but in Figure 16b shows that EHD stimulation created several new fractures that extend to the faces of the core. The fracture network in S2 after EHD-stimulation is a "V" shaped fracture network with a larger void area in the centre of the core. From the 3D x-ray CT segmentation data, and using the fracture porosity analysis method described by Ramandi et al. (2016), the theoretical fracture porosity in S2 increased from 0.34 % to 4.17 % after EHD shockwave treatment. These x-ray CT images provide evidence of the new connected, fractures in core S2 to explain why the permeability of the core increased significantly after EHD shockwave treatment. Details of the definition of fracture porosity and calculation of this property from CT-scanning slices are available in from our group's early publications (Balucan et al., 2016; Ren et al., 2018).

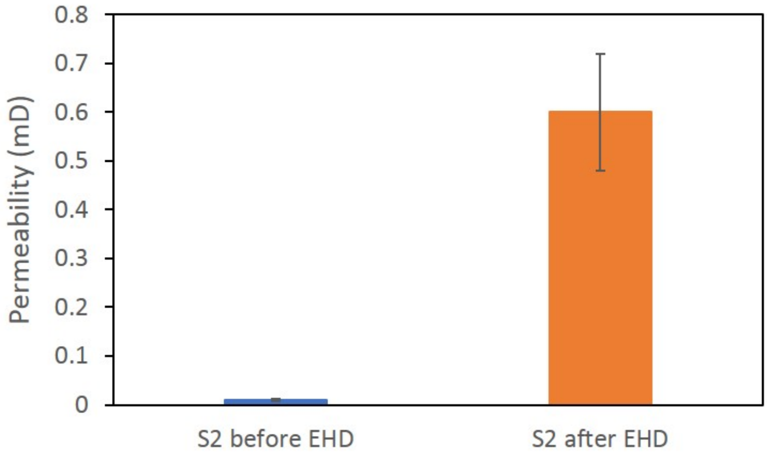

Figure 15 Change in permeability in interburden sample S2 before and after EHD stimulation fo 50 seconds at 40 pulses per second and an initial charging voltage of U_c=30 kV. Core flooding conditions of inlet pressure 10 bar, outlet pressure atmosphere, and confining pressure 20 bar.

The permeability of core S5 after EHD stimulation was not measured because the Fuji pressure film was used in the S5 EHD experiments to measure the pressure of the shockwave and this film would affect the permeability through the core. However, the development of new fractures in S5 was similar to that in S2 as shown by 3D x-ray CT void maps in Figure 16 (c) and (d). The theoretical fracture porosity in S5 increased from 0.41 % to 5.26 % after the 2000 EHD shocks (at 80 PPS for 25 seconds) with development of a “Y” shaped fracture network that propagated through the entire length of the S5 interburden plug. In addition to the 3D x-ray CT scans, further evidence of the development of pores and fractures in interburden samples S2 and S5 is provided in the MIP derived pore size distributions shown in Figure 17. The PSD curves show that in both S2 and S5 volume of pores in both the mesopore to macropore range, and in the large fracture or aperatures increased after EHD stimulation. These MIP results are consistent with the CT scanning map changes, witnessing the increment of pores and fractures not only occurred at macroscopic scales but also observed at microscopic scales after EHD shock impacts.

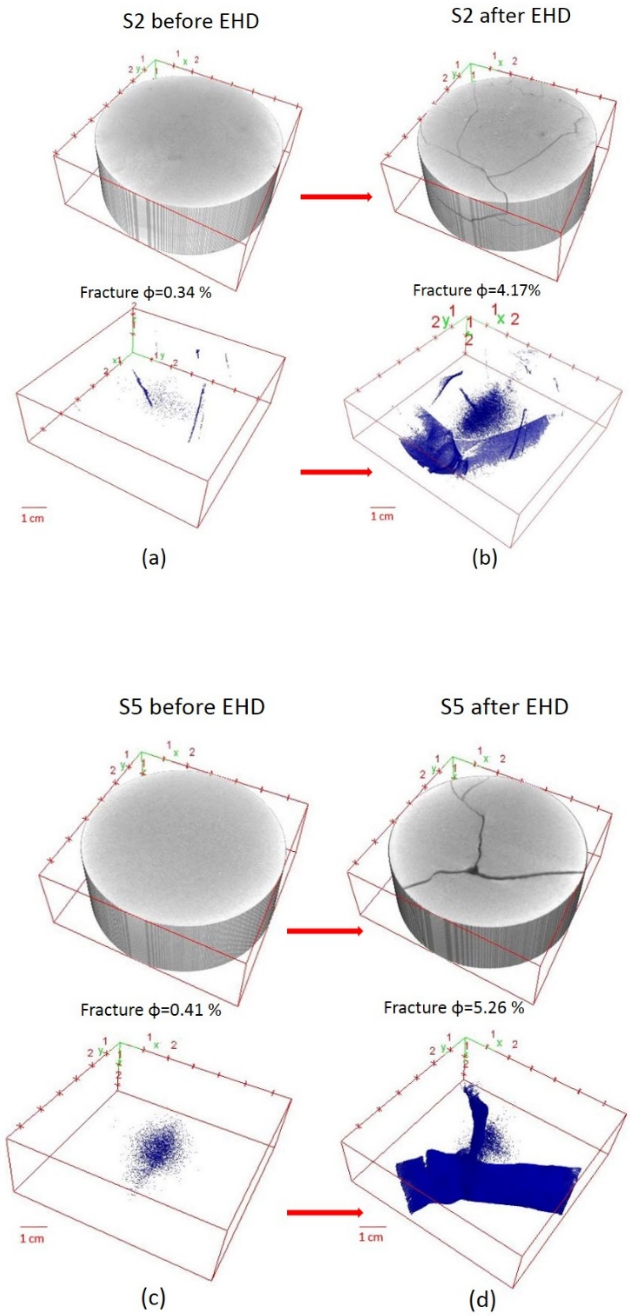

Figure 16 3D visualization of the interburden samples. (a) and (b): S2 before and after EHD stimulation (c) and (d): S5 before and after EHD with confining stress (gray=solids, black and blue=fractures or voids)

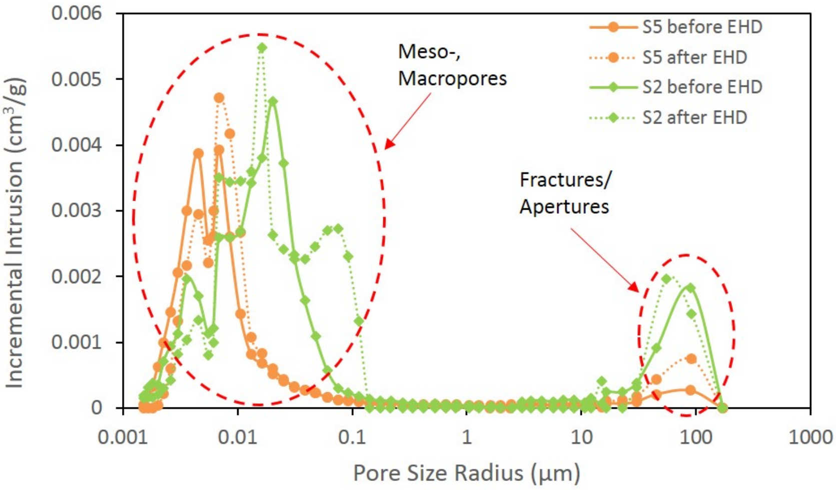

Figure 17 MIP curves for S5 and S2 before and after EHD

The stress conditions applied radially to core S5 in EHD experiment, and the pressure responses in the radial direction measured by pressure transducer PT3 and in the axial direction indicated by the Fuji film pressure sensor are shown in Figure 18. The initial confining pressure applied with the Isco pump was 20 bar, and then during stimulation significant perturbations were recorded on PT3 of up to 55.4 bar (Figure 18a) due to the shockwaves generated by EHD. Still, most of the shockwave energy was directed along the axis of the core holder with the Fuji film indicating pressure disturbance of around 32 MPa or 320 bar (Figure 18b). The resultant pressure shocks induced by EHD exceeds S5’s intrinsic compressive strength of 22.1 MPa by almost 45%, which is well in excess of the minimum required stress to fracture the rock (Gajendran et al., 2015).

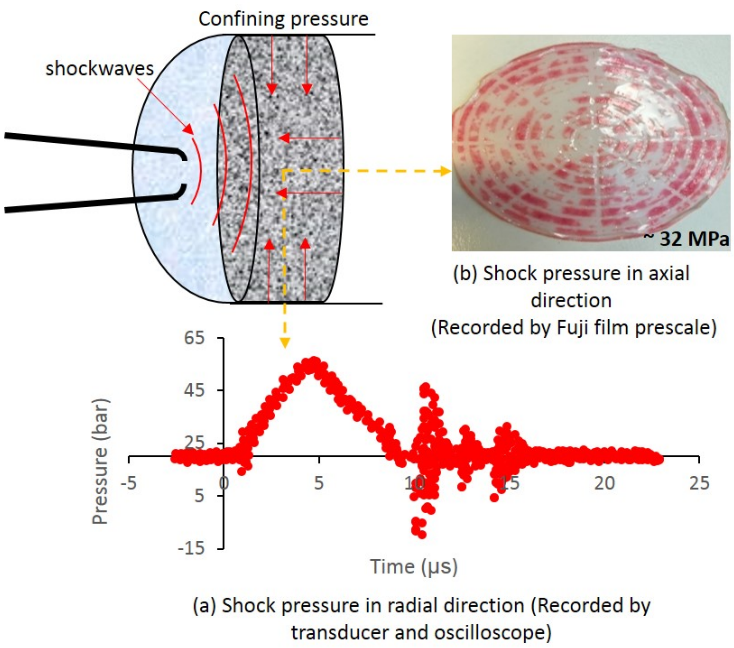

Figure 18 Pressure-recording of S5 at (a) radial and (b) axial directions during EHD stimulation

Compared to the S2 stimulation experiment, EHD stimulation of S5 resulted in wider cracks and a greater increase in fracture porosity. The difference in EHD stimulation effectiveness may be due to several factors, such as the compressive strength of each samples, the composition of the rocks, the initial porosity and fractures in the rock, and the frequency of EHD pulses. Only two rock samples were tests in these EHD experiments at a limited range of experimental conditions. Therefore, although these results indicate potential to use EHD to enhance the permeability of clay-rich mudrocks further research is required to understand the mechanisms of fracture development by EHD stimulation and to design optimised stimulation plans.

Figure 19 illustrates the key stages in EHD shockwave generation and rock fracturing after discharge, including: (1) the shockwave generated in the discharge gap propagates through the water to the rock surface; (2) the shockwave arrives at the rock surface; and (3) the shock generates compressive stress at the leeward face of the core plug with reflected shockwaves leading to . In addition to the compressive stresses, reflected shockwaves will create tensile stress on the core's leading face. The combination of these compressive and tensile forces can break aggregations of grains in rock (Andres and Biaecki, 1986), and create new voids and fractures (Yan et al., 2016a). Furthermore, a cycle of shocks may lead to dynamic wave impacts that create shear stresses which can stimulate microcracks and larger fractures in the rock if the shear stress exceeds the rock's fatigue strength (Song et al., 1994).

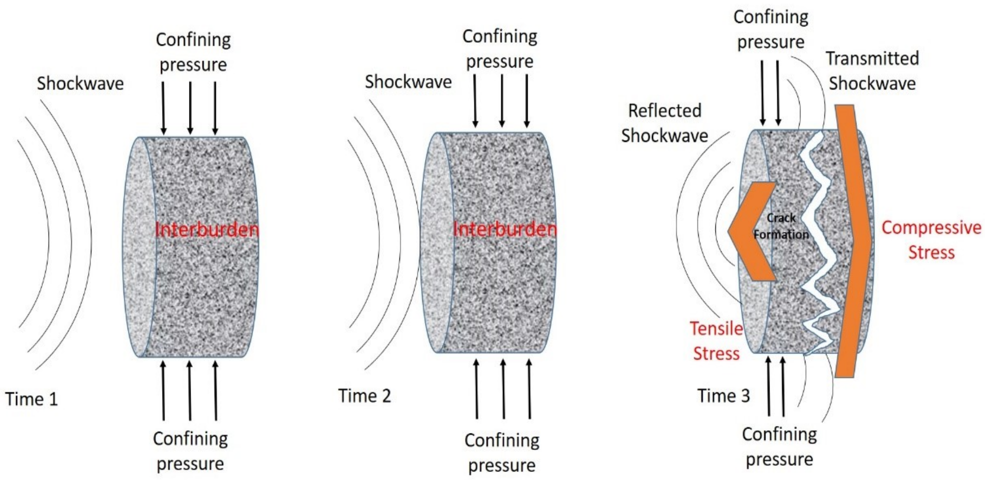

Figure 19 Conceptual schematic for the influence of shockwave on rock disaggregation

4 Conclusions

Six interburden samples were characterised in the laboratory to evaluate the potential gas storage capacity of coal seam interburden layers in the Surat Basin, and demonstrated the use of EHD stimulation as a possible method to enhance the permeability of these layers. The clay-rich mud-rocks from the interburden layers contained 0.66 wt % to 1.19 wt % total organic carbon, and this organic matter together with the microporosity of the aggregated clay-minerals provides potential for gas adsorption. The potential CH_4 storage capacity of these samples was up to about 20% of the CH_4 capacity of coals in the Surat Basin, and if there is a large cumulative thickness of the interburden layers penetrated by a CSG well these layers could contribute significantly to the total volume of gas in the reservoir.

However, the permeability of these mudrocks was very low (nano Darcies). EHD stimulation was tested as a novel fracturing technique to create new fractures and voids in two core plugs from the interburden samples, and it was observed that after EHD stimulation the permeability of S2 increased to 0.6 ± 0.11 mD. These results suggest that EHD stimulation could be a potential method to access any gas stored in coal seam interburden layers, and the method could optimised to be efficient and effective on mudrocks with different mechanical properties. Further research and development of EHD stimulation methods is required to advance these technologies.

Acknowledgements

This research was funded by the Australia Research Council Discovery Project (DP150103467). F. Ren was sponsored by a UQI scholarship, and a Top-up stipend from the UQ Centre for Coal Seam Gas (www.ccsg.uq.edu.au). The authors would like to thank Dr. Keith Hoffman and Dr. Jalil Yaghoobi for their kind help in EHD equipment assembly, commissioning and operations. X-ray CT performed at the UQ Centre for Advanced Imaging (CAI) is gratefully acknowledged.

References

Ajalloeian, R. and Lashkaripour, G.R., 2000. Strength anisotropies in mudrocks. Bull Eng Geol Env, 59: 195–199.

Andres, U. and Biaecki, R., 1986. Libertion of mineral constituents by high-voltage pulses. Powder Technology, 48: 269-277.

Arami-Niya, A., Rufford, T.E., Birkett, G. and Zhu, Z., 2017. Gravimetric adsorption measurements of helium on natural clinoptilolite and synthetic molecular sieves at pressures up to 3500 kPa. Microporous and Mesoporous Materials, 244: 218-225.

Arami-Niya, A., Rufford, T.E. and Zhu, Z., 2016. Activated carbon monoliths with hierarchical pore structure from tar pitch and coal powder for the adsorption of CO_2, CH_4 and N_2. Carbon, 103: 115-124.

Aylmore, L.A.G., 1973. Gas sorption in clay mineral systems. Clays and Clay Minerals, 22: 175-183.

Bacon, C.A., Calver, C.R., Boreham, C.J., Leaman, D.E., Morrison, K.C., Revill, A.T. and Volkman, J.K., 2000. The petroluem potential on onshore Tasmania a review. Mineral Resources Tasmania(ISBN 0 7246 4014 2).

Balucan, R.D., Turner, L.G. and Steel, K.M., 2016. Acid-induced mineral alteration and its influence on the permeability and compressibility of coal. Journal of Natural Gas Science and Engineering, 33: 973-987.

Bieniavski, Z.T., 1968. The effect of specimen size on compressive strength of coal. Int. J. Rock Mech. Min., 5: 325-335.

Broichhausen, H., Littke, R. and Hantschel, T., 2005. Mudstone compaction and its influence on overpressure generation, elucidated by a 3D case study in the North Sea. International Journal of Earth Sciences, 94(5-6): 956-978.

Burra, A. and Esterle, J., 2011. Guidelines for the Implementation of NGER Method 2 or 3 for Open Cut Coal Mine Fugitive GHG Emissions Reporting (C20005) and Technical Discussion of the Implementation of NGER Method 2 or 3 for Open Cut Coal Mine Fugitive GHG Emissions Reporting (C20005A). Final Report ACARP C20005. Brisbane, Australia: ACARP (Australian Coal Industry Research Program).

Bustin, A.M.M. and Bustin, R.M., 2016. Contribution of non-coal facies to the total gas-in-place in Mannville coal measures, Central Alberta. International Journal of Coal Geology, 154-155: 69-81.

Chen, S., Han, Y., Fu, C., Zhang, h., Zhu, Y. and Zuo, Z., 2016. Micro and nano-size pores of clay minerals in shale reservoirs: Implication for the accumulation of shale gas. Sedimentary Geology, 342: 180-190.

Dumbleton, M.J. and West, G., 1966. Some factors affecting the relationship between the clay minerals in soil and their plasticity. Clay Minerals, 6: 179-193.

Ewhurst, D.N., Aplin, A.C. and Sarad, J.P., 1999. Influence of clay fraction on pore-scale properties and hydraulic conductivity of experimentally compacted mudstones. Journal of Geophysical Research, 104(B12): 29261.

Exon, N.F., 1976. Geology of Surat Basin. Department of National Resrouces, Bureau of Mineral Resourcs, Geology and Geophysics.

Fu, X., Qin, Y., Wang, G.G.X. and Rudolph, V., 2009. Evaluation of coal structure and permeability with the aid of geophysical logging technology. Fuel, 88(11): 2278-2285.

Gajendran, K.A., Anuradha, R. and Venkatasubramani, G.S., 2015. Studies on relationship between compressive and splitting tensile strength of high performance concrete. ARPN Journal of Engineering and Applied Sciences, 10(14): 6151-6156.

Gamson, P., BEAMISH, B. and JOHNSON, D., 1996. Coal microstructure and secondary mineralization their effect on methane recovery. Coalbed Methane and Coal Geology, 109: 165-179.

Gandossi, L., 2013. An overview of hydraulic fracturing and other stimulation technologies. JRC Technical Reports.

Gandossi, L., 2016. State of the art report on waterless stimulation techniques for shale formation. Joint Research Centre (JRC).

Ge, L., Hamilton, C., Febrina, R.T., Rudolph, V. and Rufford, T.E., 2018. A phase inversion polymer coating to prevent swelling and spalling of clay fines in coal seam gas wells. International Journal of Coal Science & Technology.

Ghosal, R. and Smith, D.M., 1996. Micropore characteriation using the Dubinin-Astakhov equation to analyze high pressure CO2 (273 K) adsorption data. Journal of porous materials, 3: 247-255.

Grimes, C.E., Kestin, J. and Khalifa, H.E., 1979. Viscosity of aqeuous KCL solutions in the temperature range 25-150 ℃and the pressure range 0-30 MPa. Journal of Chemical and Engineering Data, 24(2): 121-126.

Guo, D. and Guo, X., 2017. The influence factors for gas adsorption with different ranks of coals. Adsorption Science & Technology: 026361741773018.

Hamilton, S.K., ESTERLE, J.S. and GOLDING, S.D., 2012. Geological interpretation of gas content trends, Walloon Subgroup, eastern Surat Basin, Queensland, Australia. International Journal of Coal Geology, 101: 21-35.

Hamilton, S.K., Esterle, J.S. and Sliwa, R., 2014. Stratigraphic and depositional framework of the Walloon Subgroup, eastern Surat Basin, Queensland. Australian Journal of Earth Sciences, 61(8): 1061-1080.

Langmuir, I., 1918. The adsorption of gases on plane surfaces of glass, mica and platinum. Journal of the American Chemical Society, 40: 1361-1403.

Liu, D., Yuan, P., Liu, H., Li, T., Tan, D., Yuan, W. and He, H., 2013. High-pressure adsorption of methane on montmorillonite, kaolinite and illite. Applied Clay Science, 85: 25-30.

Martin, M.A., Wakefield, M., M. K. MacPhai and al., e., 2013. Sedimentology and stratigraphy of an intra-cratonic basin coal seam gas play: Walloon Subgroup of the Surat Basin, eastern Australia. Petroleum Geoscience, 19(1): 21-38.

Mastalerz, M., He, L., Melnichenko, Y.B. and Rupp, J.A., 2012. Porosity of Coal and Shale: Insights from Gas Adsorption and SANS/USANS Techniques. Energy & Fuels, 26(8): 5109-5120.

Mcdaniel, B.W., 2005. Review of current fracture stimulation techniques for best economics in multilayer, low-permeability reservoirs. Society of Petroleum Engineers, SPE 98025.

Mines, D.o.N.R.a., 2015. Queensland's Petroleum and Coal Seam Gas.

Neuzil, C.E., 1994. How permeable are clays and shales. U.S. Geological Survey, Reston, Virginia, 30(2): 145-150.

Perera, M.S.A., RANJITH, P.G., CHOI, S.K. and al., e., 2010. A review of coal properties pertinent to carbon dioxide sequestration in coal seams: with special reference to Victorian brown coals. Environmental Earth Sciences, 64(1): 223-235.

Potter, P.E., J.B.Maynard and Depetris, P.J., 2005. Mud and mudstones. ISBN 3-540-22157-3 Springer BerlinHeidelberg New York.

Qi, L., Tang, X., Wang, Z. and Peng, X., 2017. Pore characterization of different types of coal from coal and gas outburst disaster sites using low temperature nitrogen adsorption approach. International Journal of Mining Science and Technology, 27(2): 371-377.

Ramandi, H.L., Mostaghimi, P., Armstrong, R.T., Saadatfar, M. and Pinczewski, W.V., 2016. Porosity and permeability characterization of coal: a micro-computed tomography study. International Journal of Coal Geology, 154-155: 57-68.

Rao, M.S., Bhaskar, G.U. and Karekal, S., 2015. Estimation of Uniaxial Compressive Strength of Coal Measures of Pranhita-Godavari Valley, India Using Sonic Logs. 2015 Coal Operators' Conference, The University of Wollongong: 36-47.

Ren, F., Ge, L., Rufford, T.E., Xing, H. and Rudolph, V., 2018. Permeability enhancement of coal by chemical-free fracturing using high-voltage electrohydraulic discharge. Journal of Natural Gas Science and Engineering, 57: 1-10.

Ross, D.J.K. and Bustin, R.M., 2007. Shale gas potential of the Lower Jurassic Gordondale Member, northeastern British Columbia, Canada. Bulletin of Canadian Petroleum Geology, 55(1): 51-75.

Ross, D.J.K. and Bustin, R.M., 2009. The importance of shale composition and pore structure upon gas storage potential of shale gas reservoirs. Marine and Petroleum Geology, 26(6): 916-927.

Ross, D.J.K. and Marc, B.R., 2009. The importance of shale composition and pore structure upon gas storage potential of shale gas reservoirs. Marine and Petroleum Geology, 26(6): 916-927.

Ryan, D.J., Hall, A. and Erriah, L., 2012. The Walloon Coal Seam Gas Play, Surat Basin, Queensland. APPEA Journal 52.

Saeidi, N. and Parvini, M., 2015. Accuracy of Dubinin-Astakov and Dubinin-Raduchkevic adsorption isotherm models in evaluating micropore volume of bontonite. Periodica Polytechnica Chemical Engineering, 60(2): 123-129.

Schettler, P. and Parmoly, C., 1990. The measurement of gas desorption isotherms for Devonian shale. GRI Devonian Gas Shale Technology Review, 7(1): 4-9.

Scott, S., Anderson, B., Crosdale, P., Dingwall, J. and Leblang, G., 2007a. Coal petrology and coal seam gas contents of the Walloon Subgroup — Surat Basin, Queensland, Australia. International Journal of Coal Geology, 70(1–3): 209-222.

Scott, S., Runge, C., Ross, T. and Stackhouse, Z., 2007b. How much methane gas can shales contribute to a producing coal seam gas well.

Scott, S.G., 2008. The geology, stratigraphy and coal seam gas characteristics of the Walloon subgroup- northeastern Surat Basin. PhD thesis from James Cook University.

Shneider, J., FLEMINGS, P.B., STIRRAT, R.J. and GERMAINE, J.T., 2011. Insights into pore-scale controls on mudstone permeability through resedimentation experiments. Geology, 39(11): 1011-1014.

Sing, K.S.W., Everett, D.H., Haul, R.A.W., Moscou, L., Pierotti, R.A., Rouquerol, J. and Siemieniewska, T., 1985. Reporting physisorption data for gas/solid systmes with special reference to the determination of surface area and porosity. Pure & Appl. Chem., 57(4): 603-619.

Song, J., Chen, J. and Liu, B., 1994. Study and test of enhanced oil recovery technique using low frequency pulse wave. Oil Drilling and Production Technology, 16(6): 81-87.

Tang, S. and Fan, Z., 2014. Methane adsorption characteristics of clay minerals in organic-rich shales. Journal of China Coal Society, 39: 1700-1706.

Yan, B.N., Zhou, J., Zhao, L., Liu, C. and Mengd, F., 2016a. Experimental Study on the Discharging characteristics of pulsed high-voltage discharge technology in oil plug removal. Journal of Power Technologies, 96(4): 261-268.

Yan, F., Lin, B., Zhu, C., Zhou, Y., Liu, X., Guo, C. and Zou, Q., 2016b. Experimental investigation on anthracite coal fragmentation by high-voltage electrical pulses in the air condition: Effect of breakdown voltage. Fuel, 183: 583-592.

Yang, Y.L. and Apin, A.C., 2004. Definition and practical application of mudstone porosity-effective stress relationshiops. Petroleum Geoscience, 10: 153-162.

Yang, Y.L. and Aplin, A.C., 2010. A permeability–porosity relationship for mudstones. Marine and Petroleum Geology, 27(8): 1692-1697.

Yu, W., Sepehrnoori, K. and Patzek, T.W., 2014. Evaluation of Gas Adsorption in Marcellus Shale. Journal of Society of Petroleum Engineers, SPE-170801-MS.

Zhang, T., Ellis, G.S., Ruppel, S.C., Milliken, K. and Yang, R., 2012a. Effect of organic-matter type and thermal maturity on methane adsorption in shale-gas systems. Organic Geochemistry, 47: 120-131.

Zhang, Z., Zeng, X., Wang, Y. and Cai, Q., 2012b. Experimental study of the focusing property of underwater pulsed discharge shock wave. Journal of national university of defense technology, 34(4): 54-57.